Interpretation of force and acceleration signals during hammer impact in SPT tests.

Juliana Azoia Lukiantchuki & Edmundo Rogerio Esquivel
Department of Geotechnical Engineering - University of Sao Paulo, Sao Carlos, Sao Paulo, Brazil
George de Paula Bernardes
Department of Civil Engineering – State University of Sao Paulo, Guaratingueta, Sao Paulo, Brazil

ABSTRACT
The Standard Penetration Test (SPT) is a test which provides assessment of soil properties and foundation design parameters. The SPT-N value depends not only on the soil properties and the SPT sampler characteristics, but also on the energy delivered to the rod string and SPT sampler during the hammer impact. This amount of energy can be assessed by monitoring normal forces and accelerations acting in the sampler during the hammer blow. The aim of this work is to show the analysis and the interpretation of force and acceleration signals obtained during a hammer impact in SPT tests. For this purpose, a suitable instrumented subassembly was designed, constructed and used in field tests. Tests were performed with the instrumented subassembly placed below the anvil and just above the sampler. The energy transferred to string of rods in SPT tests was evaluated through analyses of acceleration and force signals. Hamilton's principle was used to evaluate the work needed to penetrate the sampler into the soil. This method showed close agreement with the Force-Velocity method when the instrumentation was placed above the sampler.

PRESENTACIONES TÉCNICAS
El ensayo de penetración estándar (SPT) es un tipo de sondeo que permite evaluar las propiedades del suelo y los parámetros para diseño de cimentaciones. El valor de SPT-N no sólo depende de las propiedades del suelo y de las características del tomamuestras o cuchara normal SPT, también depende de la energía entregada al varillaje y a la cuchara durante el impacto del martillo. Esta cantidad de energía puede ser evaluada mediante el seguimiento de las fuerzas normales y aceleraciones que actúan en la cuchara durante el golpe de martillo. El objetivo de este trabajo es mostrar el análisis y la interpretación de los registros de fuerza normal y aceleración en la cuchara, obtenidos durante un impacto de martillo. Los resultados de las pruebas de SPT mostraron la conveniencia de la barra instrumentada para evaluar la cantidad de energía que llega a la cuchara. Las pruebas se realizaron con la barra instrumentada posicionada inmediatamente después de la cabeza de golpeo y justo arriba de la cuchara. La energía transferida a la cadena de barras y a la cuchara se evaluó mediante el análisis de los registros de aceleración y fuerza normal. El principio de Hamilton fue utilizado para evaluar los trabajos necesarios para penetrar la cuchara en el suelo. Este método ha demostrado tener una estrecha concordancia con el método de fuerza-velocidad, cuando la instrumentación se colocó justo arriba de la cuchara.

1 INTRODUCTION

The Standard Penetration Test (SPT) is the most widely used tool in the Americas for geotechnical subsurface investigation. This test provides assessment of soil properties and foundation design parameters.

The above mentioned test consists of driving a standard sampler into the soil at the bottom of a borehole. It is performed using repeated blows of a 63.5 kg (65 kg in Brazil) hammer falling through 760 mm (750 mm in Brazil). For each hammer drop there is a corresponding potential energy (E_P) that is theoretically equal to 474.5 J (478.2 J in Brazil).

The N_{SPT} index is the number of blows required to achieve a penetration of 300 mm, after an initial seating drive of 150 mm. The N_{SPT} index depends not only on the soil properties and on the SPT sampler characteristics, but also on the energy delivered to the rod string and SPT sampler during the hammer impact. Due to energy losses in the different mechanical components of the hammer release system and other sources of dissipation, the energy delivered to the rods and sampler is not equal to the theoretical potential energy. The amount of energy delivered to the top of the rod string that is transmitted to the sampler is significantly influenced among other factors, by the hammer efficiency, by the length and the mass of the rods between the anvil and the sampler and by the soil conditions.

Thus, the assessment of the energy delivered to the rod string and sampler is of great importance. The efficiency of the SPT equipment is usually defined as the ratio of actual energy transferred to the drill rods to theoretical potential energy.

The energy transferred to the drill rods is evaluated from accelerations and normal forces measured during the hammer impact (Howie *et al*, 2003; Odebrecht, 2005; Belincanta, 1998; Cavalcante, 2002). In conventional methods, the accelerations and normal forces are measured just below the anvil, through an instrumented subassembly installed next to the top of the string of rods (Figure 1).

However, according to the SPT efficiency redefinition, proposed by Aoki and Cintra (2000), the actual energy that reaches the sampler should be evaluated. For this reason, the instrumented subassembly should be placed just above the sampler. This fact motivated the development of a suitable instrumented subassembly, to be mounted just above the sampler, for reading

acceleration and force signals just above the sampler, similar to what was done by Odebrecht (2005) and Cavalcante (2008) (Figure 2). Thus, the main purpose of this research is to assess the energy that is delivered to the sampler, through analysis, interpretation and understanding of accelerometers and load cell signals collected during the hammer impact.

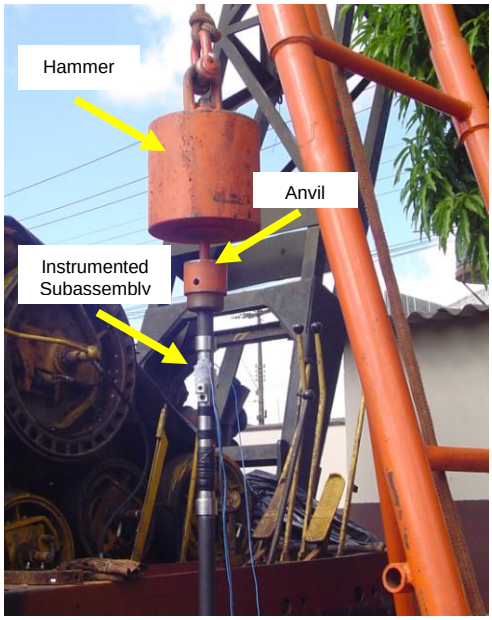

Figure 1. Instrumented subassembly placed below the anvil.

Figure 2. Instrumented subassembly placed above the sampler.

2 INSTRUMENTATION

2.1 Instrumented Subassembly

In this research, the developed instrumented subassembly consists of one rod segment in which two accelerometers and one load cell are mounted (Figure 3), similar to the one developed by Odebrecht et al (2005). The rod segment, which was made of martensitic stainless steel (VC – 150), received a heat treatment to improve its strength characteristics. The resulting yield stress was 1084 MPa while the predicted maximum stress is about 365 MPa for the foreseeing tests.

2.2 Load Cell Electrical Circuit

The load cell electrical circuit is based on a Wheatstone bridge, composed of four double strain gauges (350 Ω each) assembled 90° apart (Figure 4a). The strain gauges have been fixed with cyanoacrylate adhesive and protected with epoxy resin.

2.3 Accelerometers

A pair of PCB Piezotronics piezoelectric accelerometers (model 350B04) was rigidly mounted on the rod segment (Figure 4b). These accelerometers are capable of measuring accelerations up to 5000 g, in the 0.4-10000 Hz frequency range. The complete instrumentation is shown in Figure 5.

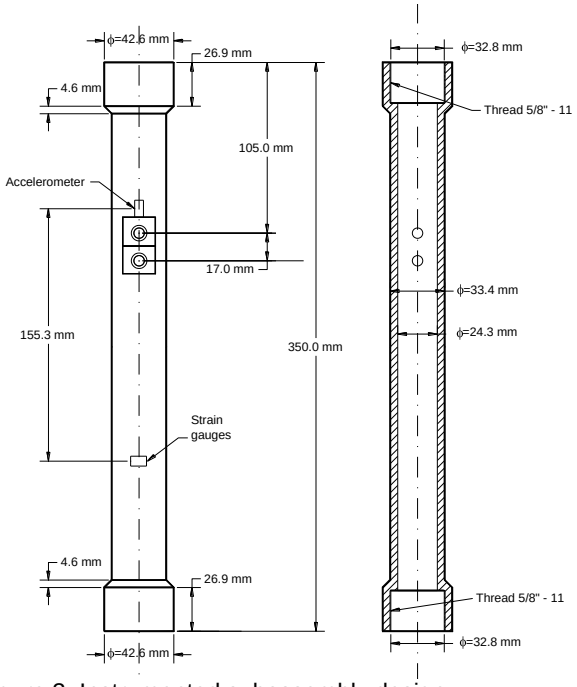

Figure 3. Instrumented subassembly design.

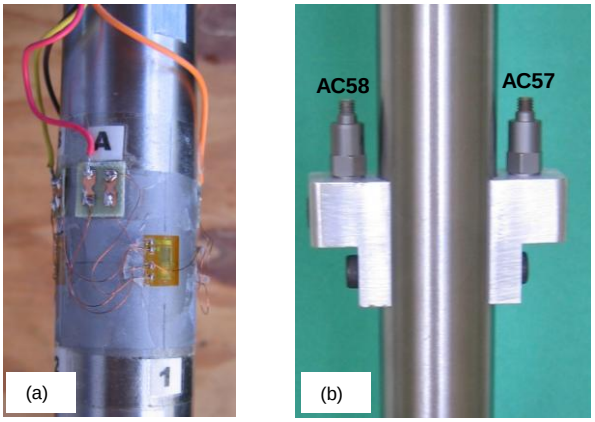

Figure 4. Instrumentation: (a) load cell and (b) accelerometers.

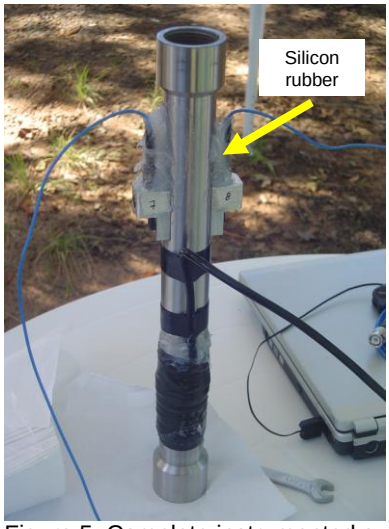

Figure 5. Complete instrumented subassembly.

2.4 Data Acquisition System

An HBM data acquisition system, model MX 410 (Figure 6), was used to record the signal data. This four-channel portable data acquisition system is suitable for analyzing high frequency dynamic events. It is capable of sampling at 96 kHz rate per channel with a resolution of 24 bits. Sampling rates and filters can be independently adjusted for each channel. This equipment is able to supply adjustable transducer excitation (DC) in the 5–24 V range. For recording acceleration signals, it was necessary to use special IEPE (Integral Electronic Piezoeletric) signal conditioners, in order to amplify the signals during the data acquisition.

2.5 Data Acquisition Procedures

The signals were collected and monitored using the Catman Easy 3.0 software, which enables graphic visualization of the collected data in real time. Through this software, it is possible to fully configure the data acquisition system, providing transducer calibration information, selecting the sampling rate, activating the triggering system and adjusting the cut-off frequency of the low pass filter, among many other features.

The accelerometer calibration data was obtained from the chart provided by PCB Piezotronics. A calibration equation was used for the load cell. This calibration was obtained through static load tests performed at the University of Sao Paulo laboratories. Field tests were conducted at a 96 kHz sampling rate per channel. Additionally, a trigger, a pre-trigger and a low pass filter (anti-aliasing), corresponding to 15% of the selected sampling rate, were used.

During the hammer impact, data signals could be graphically visualized in real time (Figure 7). After the data acquisition had been completed using the Catman Easy software in analysis mode, the data could be evaluated, treated and filtered.

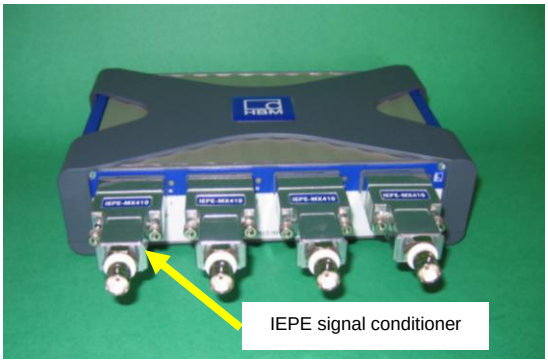

Figure 6. HBM data acquisition system.

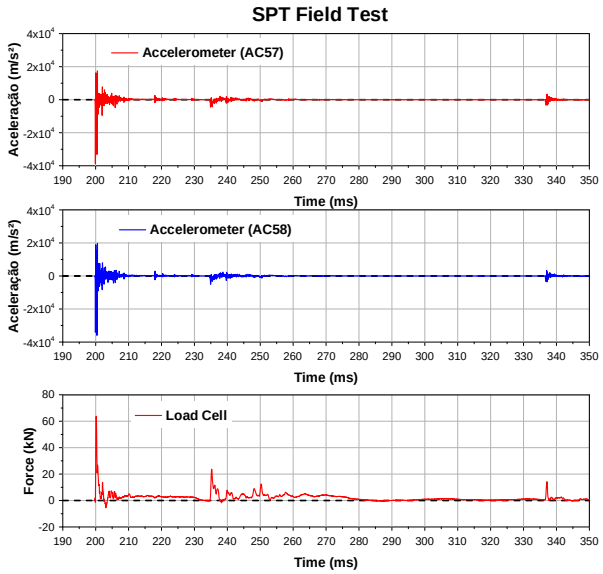

Figure 7. Force and acceleration typical signals.

3 FIELD TESTS

3.1 SPT Field Test Procedures

The SPT field tests, carried out according to the ABNT (2001) Brazilian Standard, were conducted at the Experimental Research Site of the University of Sao Paulo and at a field site in Ribeirao Preto.

As positioning the instrumentation just above the sampler leads to extra difficulties, it was necessary to take some safety measures. First, the borehole was drilled with a diameter of 100 mm to provide enough room for the instrumented subassembly. Second, holes were lined with PVC tubes, to prevent their closure and protect the instrumentation. Finally, the accelerometers were protected with a thick silicon rubber layer.

4 CALCULATIONS AND ANALYSIS PROCEDURES

4.1 Calculations and Analysis

Velocity data were obtained by integrating the acceleration signals. In this procedure, it was assumed that at the initial instant, the acceleration and the time were equal to zero. Likewise, velocity data were corrected, setting to zero the initial calculated

velocity. Velocity data can be converted to force units using Equation 1.

$$F(t) = \frac{A \times E}{c} \times v(t) = Z \times v(t) \quad [1]$$

where A = area of the rod cross section (4.1×10^{-4} m^2); E = modulus of elasticity of the rod (206840 MPa); c = theoretical wave propagation velocity = $(E/\rho)^{0.5}$ = 5120 m/s; ρ = mass density of the rod (7880 kg/m3); v = particle velocity; Z = rod impedance (Sancio and Bray, 2005).

The energy was obtained by integrating the product force times velocity with respect to time (Eq. 2). The initial integration instant (t_i) corresponds to the beginning of the event (force value different from zero) and the final integration instant (t_f) is when the force becomes zero and no subsequent impacts are observed. The force-velocity integration method (FV) for evaluating the STP energy is a theoretically more consistent approach than the force integration method (F^2). The FV method provides the correct SPT energy even when the proportionality between force and velocity is lost (Howie et al., 2003).

$$E = \int_{t_i}^{t_f} F(t) \times v(t) dt \quad [2]$$

4.2 Application of Hamilton's Principle to the SPT Constant Energy Dynamic Loading Test.

Hamilton's principle was introduced to SPT test analyses by Aoki and Cintra (2000). These authors consider the application of Hamilton's principle to the time interval (t_2 - t_1), where t_1 is the instant when a compression wave arrives to the top of the rod-sampler-soil system, and t_2 is the instant corresponding to the end of the hammer impact, when all the kinetic energy had been dissipated.

Figure 8 shows a typical displacement-resistance curve corresponding to a section at the top of rod-sampler-soil system.

Figure 8 shows the maximum downwards displacement (ρ_{max}) and the corresponding maximum mobilized resistance (Rt) (point B). At this instant, the velocity becomes zero and the kinetic energy (T) is transformed into potential deformation energy (V), which is accumulated in the rod-sampler-soil system. Other energies losses are not taken into account.

$$V = T = T_0 \quad [3]$$

In this figure, the potential deformation energy accumulated in the rod-sampler-soil system is numerically equal to the area OBCO (Figure 8). At the end of hammer impact (point D), the potential deformation energy is transformed into work done by non-conservative forces and into elastic recoverable energy (W_{nc}).

$$V = W_{nc} + V_e \quad [4]$$

where V = potential energy in the system, W_{nc} = work done by non-conservative forces including damping (area OBDO) and V_e = elastic recovery energy (area BCDB).

At the time t_2 after the unloading, it is possible to record the displacement components due to the elastic and permanent deformations.

$$\rho_{max} = \rho_e + \rho_p \quad [5]$$

where ρ_{max} = maximum downwards displacement, ρ_e = recovered elastic displacement and ρ_p = permanent sampler penetration.

In the case of inelastic and very low resistant soil below the sampler, the applied kinetic energy will be transformed into work done in the sampler – soil system, during the permanent sampler penetration (Aoki and Cintra, 2000).

$$\rho_{max} = \rho_p \quad [6]$$

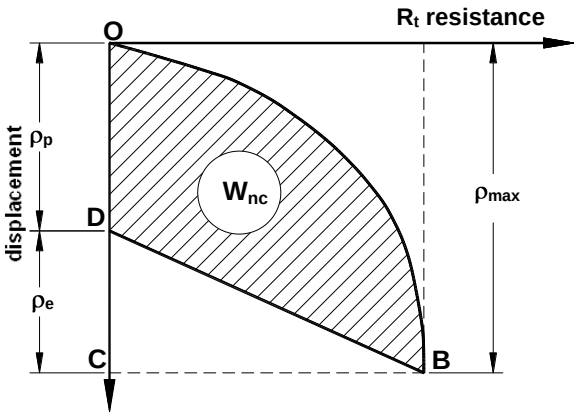

Figure 8. Displacement versus resistance curve at the top of rod-sampler-soil system (Aoki and Cintra, 2000).

Moreover, in this case the elastic soil deformation energy can be neglected and almost all kinetic energy transformed into work done during the permanent penetration of the sampler into the soil, resulting:

$$V = W_{nc} \quad [7]$$

5 SPT RESULTS

5.1 Force and acceleration signals

5.1.1. Instrumentation below the anvil

Figures 9 and 10 show acceleration and force signals, which were obtained from testes performed at the Ribeirão Preto site. These figures also show force and velocity times rod impedance curves, energy and corrected energy ratio curves. Corrected energy ratio is defined as the ratio between the actual energy reaching the sampler and the potential energy delivered to the soil.

The records shown in Figure 9 and Figure 10 correspond to the first and the third blows, respectively, using a 6.65-meter long string of rods. In the above mentioned graphs, the first and the secondary impacts are evident. To take into account the sampler penetration

and the rod weight effects, the potential energy has to be corrected. This correction was performed according to the Odebrecht et al. (2005) approach (Eq. 8):

$$E^* = E_p + (M_h + M_r) \times g \times \rho \qquad [8]$$

where E^* = potential energy delivered to the soil; E_p = nominal potential energy (478 Joules for the Brazilian SPT); M_h = hammer weight; M_r = rod weight; g = acceleration of gravity; ρ = sample penetration caused by one blow.

Accelerations are higher after the sampler penetrates the soil. However, it was observed that the measured accelerations were compatible with the capacity of the accelerometers. Thus, the instrumentation developed is suitable to measure the energy that enters the drill rods.

5.1.2. Instrumentation above the sampler

Figures 11 and 12 show acceleration and force signals, which were obtained from tests performed at the Sao Carlos site. These figures also show force and velocity times rod impedance curves, energy and corrected energy ratio curves.

The records shown in Figure 11 and Figure 12 correspond to the first and the third blows, respectively, using a 6.35-meter long string of rods. In the Sao Carlos site, there exists a 6-m thick lateritic clayey sand layer above a pebble line. This layer is unsaturated, very porous and collapsible, showing low bearing capacity, with a N_{SPT} index ranging from 1 to 8 blows. In the above mentioned graphs, the first and the secondary impacts are evident.

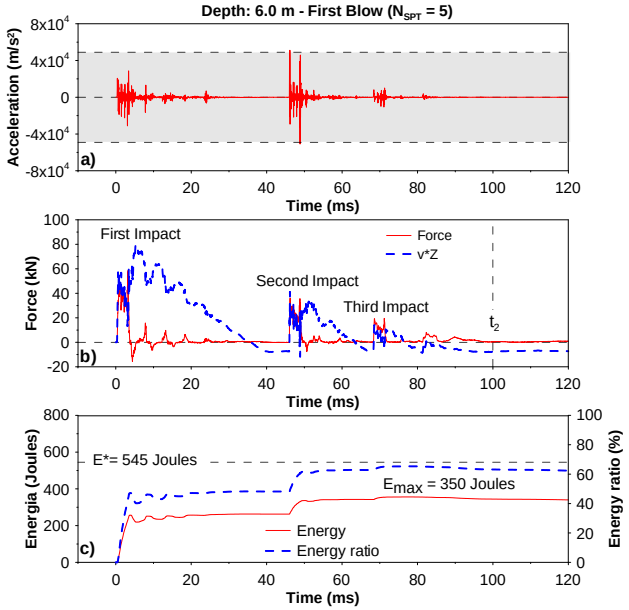

Figure 9. (a) Acceleration records, (b) Force and v*Z curves and (c) energy and corrected energy ratio curve.

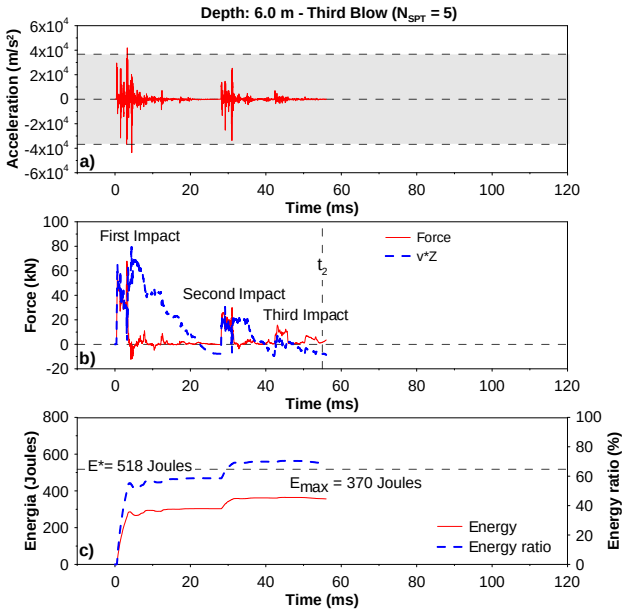

Figure 10. (a) Acceleration records, (b) Force and V*Z curves and (c) energy and corrected energy ratio curve.

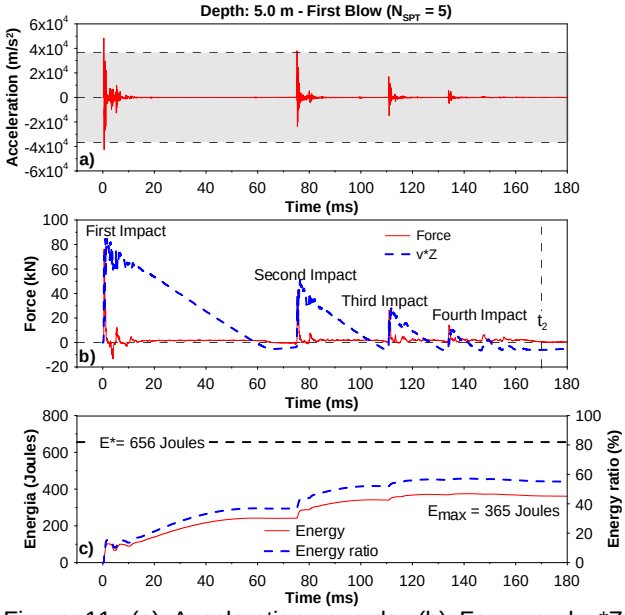

Figure 11. (a) Acceleration records, (b) Force and v*Z curves and (c) energy and corrected energy ratio curve.

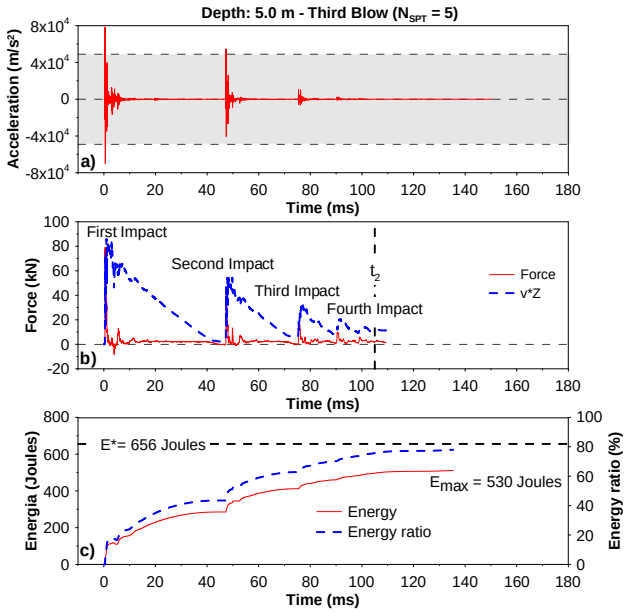

Figure 12. (a) Acceleration records, (b) Force and v*Z curves and (c) energy and corrected energy ratio curve.

The wave reflection effects could be observed during the time interval between the first and the second impacts. For low resistance soils, the reflected wave intensity (tensile wave) on the sampler is higher than the wave intensity for high resistance soils, causing a separation between the impact plan and the hammer. Consequently, there is an interruption of energy transference for a long period of time. On the other hand, for high resistance soils, the reflection wave intensity and the time interval between the first and the second impacts decrease. Consequently, less secondary impacts may occur.

The time interval between the first and second impacts decreases as the sampler penetrates the soil. This behavior can be associated with low resistance soils, mainly for the first blow (Figures 11a and 11b). In this case, the soil may be loose due to the borehole drilling operation. For the subsequent blows, as the sampler penetrates the soil, the time interval between the first and the second impact decreases (Figures 12a and 12b).

Moreover, these records also show that after the sampler starts to penetrate the soil, accelerations show a tendency to be higher than when the sampler penetration has not started yet. This was noticed by comparing the maximum accelerations for the first blow (49000 m/s^2) and for the third blow (80000 m/s^2). For this reason, the use of accelerometers model 350B04 may cause loss of part of acceleration signals. Thus, the developed instrumentation has to be improved by using accelerometers with acceleration measurement and frequency broader ranges.

The maximum values of energy, corresponding to the end of the event, are equal to 365 J and 530 J for the first and third blows, respectively. Also, the energy ratio is equal to 59% and 79% for the first and third blows, respectively. The curves showed in Figures 11 and 12 make evident the importance of secondary impacts in the total amount of energy that reaches the sampler in the case of loose soils.

SPT field test results show that when the instrumented subassembly is placed just below the anvil, the magnitudes of accelerations are lower than when it is placed just above the sampler.

In the case of the first blow in SPT tests, the tip of the sampler is free (tip resistance is null), allowing the tip to move downward. This tip movement generates a reflected tensile wave, which doubles the particle velocity at the tip of the sampler (Skov, 1982). When the instrumentation is placed just above the sampler, the time interval between the incoming compressive wave and the reflected tensile wave is very short (Figure 13). Due to the particle velocity superposition, the accelerations are added up and consequently surpass the accelerometer capacity (49000 m/s^2).

When the instrumentation is placed just below the anvil, the time interval between the instants in which the incoming compressive wave and the reflected tensile wave reach the instrumented section, respectively, is increased (Figure 13). Thus, despite the occurrence of particle velocity superposition, the recorded acceleration amplitude will not be so high because when the reflected tensile wave arrives to the section, the incoming compressive wave has already decreased. For this reason, acceleration magnitudes will be lower than when the instrumentation is placed just above the sampler.

In conclusion, for the Brazilian SPT, when the instrumentation is placed just above the sampler, it is necessary to use accelerometers capable of recording accelerations with a magnitude higher than 10000 g and frequencies up to 15000 Hz.

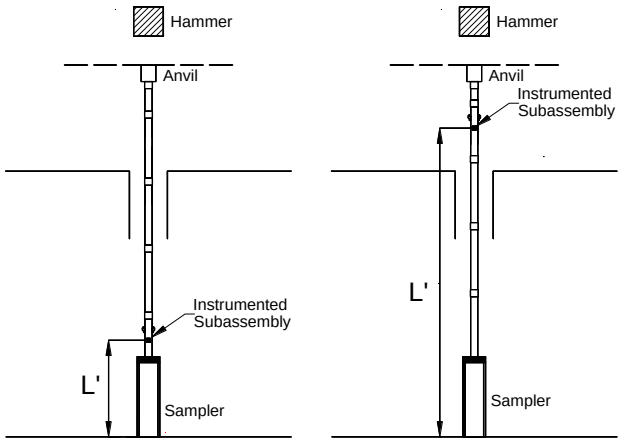

Figure 13. Time interval according to instrumented subassembly position (2L'/c).

5.2 Hamilton's Principle Application

Figure 14 shows the force and the velocity times rod impedance curves corresponding to the third blow at a depth of 4 m obtained from a test performed at the Sao Carlos site. This figure also shows the energy curve obtained through FV method.

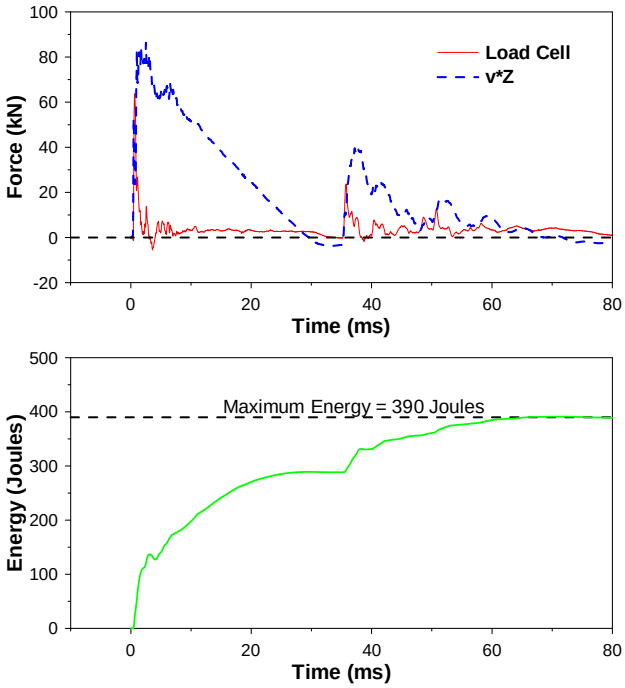

Figure 14. Force and v*Z curves (Third blow at the depth of 4 m).

Displacement data were obtained by integrating the velocity data with respect to time (Figure 15). A close agreement between the maximum displacement and the actual sampler penetration can be noticed.

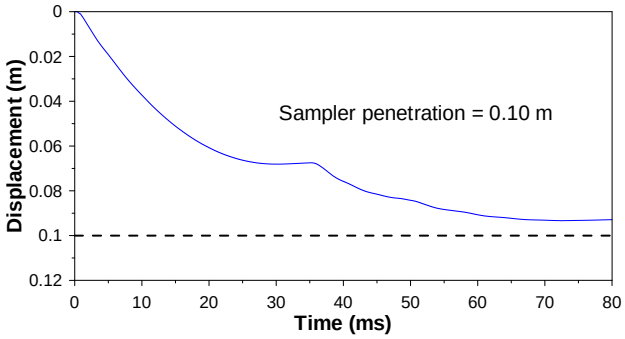

Figure 15. Displacement curve (Third blow at the depth of 4 m).

To evaluate the energy needed to penetrate the sampler into the soil, when the instrumentation is placed just above the sampler, the Hamilton's principle can also be used. According to this principle, this work is obtained through the integration of forces with respect to displacements (Aoki and Cintra, 2000).

Figure 16 shows the force versus displacement curve.

Performing a numerical integration, the calculated energy resulted in 406 J (Figure 16). This value is alike to the energy amount calculated using the FV method (390 J in Figure 14). As a matter of fact, these two values are alike. Since the difference between these two values is less than 4%, it can be concluded that the energy reaching the sampler is practically equal to the work done to penetrate the sampler into the soil, confirming that for this soil, the elastic recoverable energy (V_e) is negligible (Aoki and Cintra, 2000).

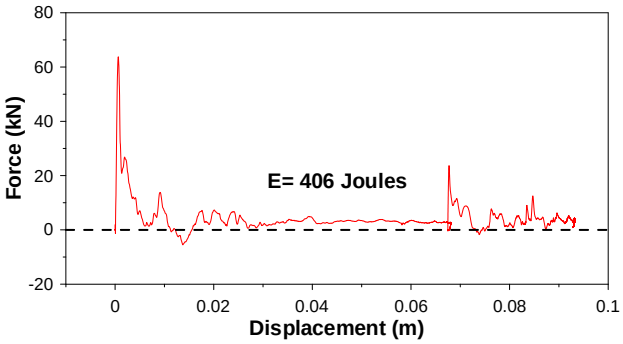

Figure 16. Force versus displacement curve (Third blow at the depth of 4 m).

The case corresponding to the third blow at the depth of 7 m is shown as follows. Figure 17 shows the force and the velocity times rod impedance curves. This figure also shows the energy curve obtained through the FV method.

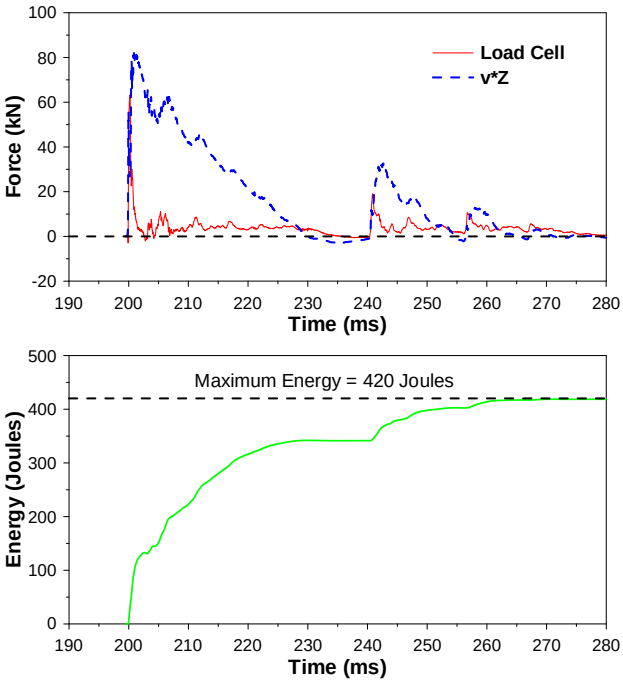

Figure 17. Force and v*Z curves (Third blow at the depth of 7 m).

Figure 18 shows the displacement curve. The maximum displacement is close to the sampler penetration. Figure 19 shows the force versus displacement curve. In this case, it is noticed that the energy value calculated by the FV method (420 J) and the one calculated through the Hamilton's principle method (434 J) are alike. The difference between these two values is about 3%.

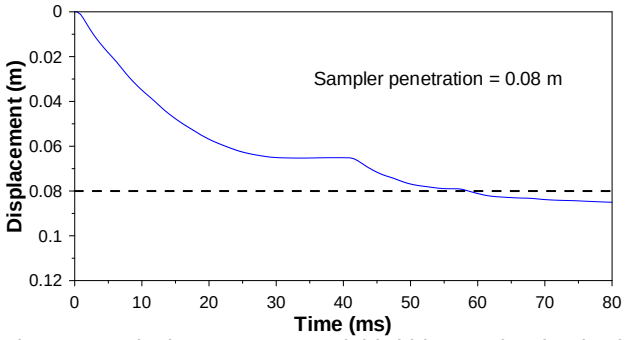

Figure 18. Displacement curve (Third blow at the depth of 7 m).

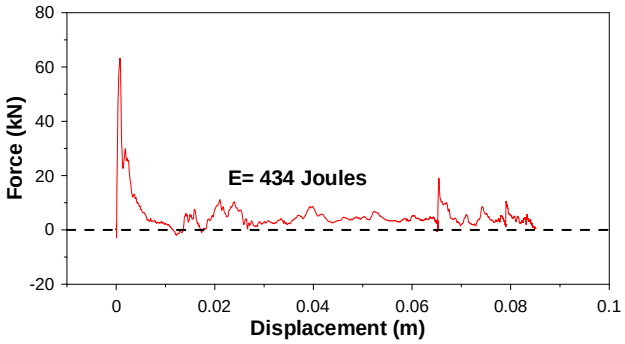

Figure 19. Force versus displacement curve (Third blow at the depth of 7 m).

6 CONCLUSION

Force and acceleration signals collected during hammer impacts in SPT tests were evaluated and interpreted. The instrumented subassembly was placed in two different positions: just above the sampler and below the anvil. From the performed analyses, the following conclusions could be stated:

1. The energy transferred to the string of rods in SPT tests can be evaluated through analyzes of acceleration and force signals.

2. The potential energy has to be corrected to take into account the sampler penetration and rod weight effects.

3. The maximum accelerations are higher when the instrumentation is placed just above the sampler than when the instrumentation is placed below the anvil.

4. After the sampler starts to penetrate the soil, accelerations show a tendency of being higher than when the sampler penetration has not started yet.

5. The secondary impacts are important in the evaluation of the total amount of energy that reaches the sampler, particularly in the case of loose soils.

6. The time interval between the first and the second impacts depends on the wave reflection effects; for low resistance soils the reflected wave intensity is higher than for high resistance soils.

7. Hamilton's principle was used to evaluate the work needed to penetrate the sampler into the soil. This method shows close agreement with FV method when the instrumentation was placed above the sampler.

8. For properly evaluating the energy reaching the sampler, when the instrumentation is placed just above the sampler, the developed instrumented subassembly should be improved with the installation of accelerometers with acceleration measurement and frequency broader ranges. However, these accelerometers can be used to evaluate the energy at the top of the drill rods because accelerations signals are lower than the acceleration signals when the instrumentation is placed above the sampler.

ACKNOWLEDGEMENT

The authors are very thankful to FAPESP (Grant No. 2008/08268-4) and CNPq (Grant No. 479001/2009-0) for the financial support. Furthermore, the first author is very thankful to CAPES for granting a scholarship that made it possible the development of this research both in Brazil and Canada.

REFERENCES

ABNT. 2001. Standard penetration test (SPT). NBR 6484, Rio de Janeiro, 17p. (In Portuguese).

Aoki, N; Cintra, J.C.A. 2000. The application of energy conservation Hamilton's principle to the determination of energy efficiency in SPT tests, *In: International conference on the application of stress waves theory to piles* 6, v.1, p. 457 – 460, Sao Paulo.

Belincanta, A. 1998. Evaluatin of intervening factors in the penetration resistance of the SPT (in Portuguese). Doctorate thesis, University of Sao Paulo, Sao Carlos, Brazil.

Cavalcante, E.H. 2002. Theoretical-experimental SPT investigation (in Portuguese). Doctorate thesis, University of Rio de Janeiro, Rio de Janeiro, Brazil.

Cavalcante, E.H; Danziger, B.R; Danziger, F.A.B. 2008. On the energy reaching the sampler during SPT. In: *The 8th international conference on the application of stress wave*. Proceedings of stress wave 2008. Lisboa, Portugal.

Howie, J.A; Daniel, C.R; Jackson, R.S; Walker, B. 2003. Comparison of energy measurement methods in the standard penetration test. Reported prepared for the U.S Bureau of Reclamation, Geotechnical Research Group, Department of Civil Engineering, The University of British Columbia, Vancouver, Canada.

Odebrecht, E; Schnaid, F; Rocha, M.M; Bernardes, G.P. 2005. Energy efficiency for Standard Penetration Test. *Journal of Geotechnical and Geoenvironmental Engineenring*, 131(10):1252 – 1263.

Sancio, R.B; Bray, J.D. 2005. An assessment of the effect of rod length on SPT energy calculations based on measured field data. *Geotechnical Testing Journal*, 28(1):1 – 9.

Skov, R. 1982. Evaluation of stress wave measurements. *DMT*, *Grumdungstechnik*, Hamburg, Germany.